PHYSICAL REVIEW B **95**, 201405(R) (2017)

Indirect experimental evidence of a persistent spin helix in H^+ implanted Li-doped ZnO by photogalvanic spectroscopy

L. Botsch,* I. Lorite, Y. Kumar,† and P. Esquinazi

Division of Superconductivity and Magnetism, Felix-Bloch Institute for Solid State Physics, University of Leipzig, Linnéstraße 5, D-04103 Leipzig, Germany

(Received 4 January 2017; revised manuscript received 8 March 2017; published 10 May 2017)

We report a large circular photogalvanic effect (CPGE) in a 2DEG created at the interface of a semiconductor/insulator homojunction at the $(10\bar{1}0)$ surface of a Li-doped ZnO microwire by low energy proton implantation. We show that the CPGE originates from the Rashba spin-orbit interaction at the interface. Our sample arrangement allows tuning the spin-orbit interaction strength by manipulating the electron spin orientation via an external magnetic field. The results of the present work obtained at 305 K indicate the experimental realization of a persistent spin helix in ZnO.

DOI: 10.1103/PhysRevB.95.201405

I. INTRODUCTION

The control of the spin degree of freedom is the key for further development of spintronic technology. In that sense the spin-orbit interaction (SOI) appears to be a possible route since it enables the manipulation of the spin in semiconductors. It is known that such SOI can be achieved thanks to the Dresselhaus [1] and Rashba [2] effects in crystals lacking inversion symmetry. Microscopically, they can be explained by a bulk inversion asymmetry (BIA) or by structural inversion asymmetry (SIA) for the Dresselhaus and Rashba effects, respectively. Rashba effect can be achieved artificially by the design of heterostructures or delta doping, which produce confining potentials and two-dimensional (2D) structures (e.g., a 2DEG) that strongly depends on macroscopic properties like the crystal orientation and external applied fields.

In recent years, a growing interest has been given to 2D confined structures that exhibit Rashba SOI, as they allow us to control the coupling strength between electron spin and orbital degrees of freedom by applying an external electric field (Rashba effect). As a consequence, the SOI allows the manipulation of the electron spin by controlling their orbital movement and the electron currents by controlling their spin. This gives rise to numerous applications in the field of spin orbitronics (a subfield of spintronics that exploits the SOI), e.g., extremely enhanced spin diffusion lengths in a persistent spin helix (PSH) configuration [3–5], spin field effect transistors (SFET) [6,7], or spin-orbit qubits [8–10] to name a few examples. Photogalvanic spectroscopy is nowadays used in experiments to study Rashba coupling as well as other related effects [11–15].

Most of the research in this field (both theoretically and experimentally) was done on III-V compound semiconductor heterostructures and quantum well (QW) [16–20] structures in which a spin texture due to a persistent spin helix has been experimentally observed for zinc-blende semiconductors. On the other hand, the great advances to produce 2D structures in wurzite semiconductors has led to a rising interest. In addition, it has been shown by photogalvanic experiments that SOI is possible at the surface of [0001]-grown ZnO thin films [21] and at the interface of ZnO-based heterostructures [22]. However, this has not yet been achieved experimentally at the $(10\bar{1}0)$ surface where the formation of a persistent spin helix has been theoretically predicted recently for a hydrogenated ZnO surface [23,24]. The circular photogalvanic effect (CPGE) is a convenient method to investigate the spin texture caused by SOI [25] and has been successfully used in numerous material systems [22,26,27]. The realization of a Rashba SOI in the $(10\bar{1}0)$ plane of ZnO would lead to the formation of a spin helix with comparably small wavelength, an important criterion for the miniaturization of spintronic devices in structures such as nanowires.

In the present work we present evidence for the formation of a spin texture at the interface generated by low energy proton implantation near the surface of a Li-doped ZnO microwire. The evidence is provided by photogalvanic spectroscopy related to the Rasbha SOI at the $(10\bar{1}0)$ surface.

II. METHODS

ZnO microwires were prepared in a carbothermal process as described in a previous work [28] using pure ZnO powder (microwire ZH), ZnO powder with 3 at. % of Fe (microwire ZFH), and ZnO powder with 3 at. % of Li (microwire ZLH). The wires were grown in [0001] direction and have a diameter ranging between 500 nm and 10 μm. Once the wires were placed on Si/Si_3N_4 substrates with their c axis parallel to the substrate surface, the samples were exposed to remote hydrogen dc plasma with an implantation energy of 300 eV in parallel-plate configuration. For a detailed description of the process, see Ref. [28]. Finally, ohmic In or Au contacts were made for transport measurements.

The photoresistance was measured under UV (370 nm) illumination always applied normal to the wire's main axis [see Fig. 1(a)] at 305 K and a pressure of 10^{-2} mbar. A combination of linear polarizer and $\lambda/4$ waveplate were used to elliptically polarize the light for the polarization dependent photocurrent measurements. The photocurrents were measured using a resistance bridge applying a constant bias voltage of 300 mV while illuminating the wires until

*lukas.botsch@uni-leipzig.de

†Present address: Solid State Physics Division, Bhabha Atomic Research Centre, Mumbai 400085, India.

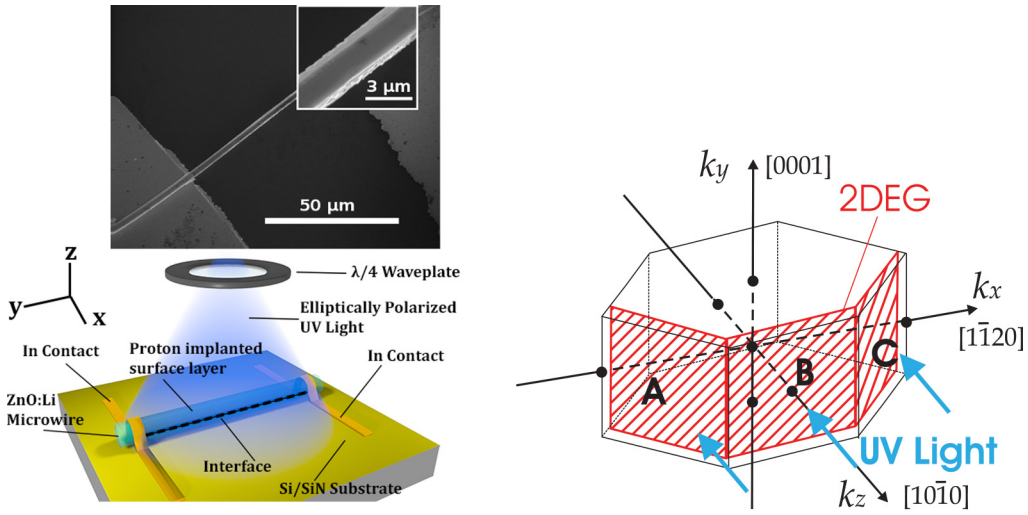

FIG. 1. (a) Sketch of the measurement method for photocurrent measurements. (b) Brillouin zone of the hexagonal ZnO lattice. The c axis ([0001] direction) is oriented in the y direction of the cubic coordinate system. The z axis is normal to the $(10\bar{1}0)$ face containing the 2DEG (in red). The UV light is irradiated along the z axis. The upper picture of the ZLH wire was obtained with a scanning electron microscope.

saturation. Saturation photocurrent values were then extracted from the photoresistance data. In this communication we show the results obtained from a 70-μm-long ZLH wire with a diameter of $\sim$3 μm.

III. RESULTS AND DISCUSSION

The photocurrent of microwires ZH, ZFH, and ZLH was measured as a function of the helicity of the elliptically polarized light by changing the angle φ between the linear polarization axis and the $\lambda/4$-waveplate axis [see Fig. 1(a)]. Figure 2 shows a clear dependence of the photocurrent as a function of φ for sample ZLH. Samples ZH and ZFH show no such dependence on the angle φ. Due to the Li doping, the intrinsic donor defects in sample ZLH are much more compensated than in the samples ZH and ZFH, which results in the formation of a 2DEG with broken inversion symmetry in a $(10\bar{1}0)$ plane near the surface after proton implantation.

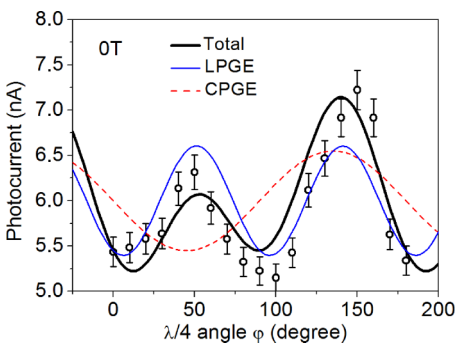

FIG. 2. Photocurrent of sample ZLH measured as a function of the angle φ of the $\lambda/4$ waveplate (circles). The thick black line represents the fit to Eq. (3) with the parameters defined in Table I. The thin dashed red line represents the CPGE contribution to the photocurrent as extracted from the fit and the thin blue line represents the LPGE contribution.

To understand the origin of the CPGE, we have to consider the spin-subband splitting due to SOI. We define the y axis of the Cartesian coordinate system along the c axis [0001] of the ZnO wire, as the direction along which the photocurrent was measured. The z axis points in the $[10\bar{1}0]$ direction [see Fig. 1(b)]. According to our previous studies [29], the formation of an interface in the $(10\bar{1}0)$ plane after proton implantation is possible. This interface parallel to the $(10\bar{1}0)$ plane reduces the symmetry of the system from the C_{6v} to the C_s point symmetry group [23]. The inversion symmetry breaking allows for the Rashba SOI. In general, the SOI Hamiltonian has the following form:

$$H_{\mathrm{SO}} = \sum_{\mu\nu} \gamma_{\mu\nu}\, \sigma_\mu\, k_\nu, \tag{1}$$

where γ is a second rank pseudotensor that characterizes the SOI strength of the system and depends on its inversion asymmetries, σ is the vector of Pauli matrices, and k is the electron momentum. According to [24], the formation of an interface in the $[10\bar{1}0]$ plane allows the linear Rashba terms γ_{zx}, γ_{yx}, and γ_{xy} to be nonzero, in this case the formation of a spin helix is predicted at the interface plane. Taking into account the system symmetry, Eq. (1) becomes

$$H_{\mathrm{SO}} = \gamma_{zx} k_x \sigma_z + \gamma_{yx} k_x \sigma_y + \gamma_{xy} k_y \sigma_x. \tag{2}$$

On the other hand, the photogalvanic effect induced current in the y direction can be described as (see Ref. [25])

$$j_y = \chi_{xy}\, \hat{e}_x\, P_{\mathrm{circ}}\, |E|^2 + \sum_{\mu,\nu} \widetilde{\chi}_{y\mu\nu}\, \frac{E_\mu E_\nu^* + E_\mu^* E_\nu}{2}, \tag{3}$$

where the first term on the right-hand side represents the CPGE and the second term the linear PGE (LPGE) contributions to the photocurrent, with E the complex amplitude of the transmitted

TABLE I. Amplitudes of the CPGE and LPGE contributions obtained by fitting Eq. (4) to the photocurrent data (see Figs. 2 and 3).

Amplitude	$B = 0$	$B = 0.4\,\mathrm{T}, B \parallel y$	$B = 0.4\,\mathrm{T}, B \parallel x$
χ_{xy} (CPGE)	0.55 nA	0.9 nA	0.1 nA
$\widetilde{\chi}_{yyy}$ (LPGE)	0.55 nA	0.55 nA	5.5 pA
$\widetilde{\chi}_{yxy}$ (LPGE)	0.25 nA	45 pA	0.2 nA

electric radiation field with components E_μ and E_ν, $\hat{e}_x$ is the x component of the unit vector pointing in the direction of light propagation, and P_{circ} is the light helicity. The pseudotensors χ and $\widetilde{\chi}$ describe the anisotropy of the CPGE and LPGE, respectively. Equation (2) and the part of Eq. (3) describing the CPGE are characterized by the same anisotropy in space [25] and therefore we can probe the SOI anisotropy by measuring the CPGE induced photocurrent.

Note that due to the factor $\hat{e}_x$, the CPGE contribution to the photocurrent requires oblique incident light on the surface plane, so that face B of the wire shown in Fig. 1(b) cannot contribute to the effect, whereas under symmetry considerations, faces A and C contribute with opposite signs. The measured CPGE induced photocurrent is therefore given by $j_y^{\mathrm{total}} = j_y^C - j_y^A$, the difference between the contributions of the two faces A and C. For simplicity, we will continue to use the coordinate system introduced above and assume oblique incidence of light on a single surface.

Equation (3) can be rewritten as a function of the angle φ of the $\lambda/4$ waveplate:

$$j_y = -E_0^2 t_s t_p \Bigg[\chi_{xy}\, \hat{e}_x \sin 2\varphi - \frac{\widetilde{\chi}_{yxx} + \widetilde{\chi}_{yyy}}{2} + \frac{\widetilde{\chi}_{yxx} - \widetilde{\chi}_{yyy}}{4}(1 + \cos 4\varphi) + \frac{\widetilde{\chi}_{yxy}}{2}\sin 4\varphi \Bigg], \quad (4)$$

with E_0 the amplitude of the electric radiation field of the light source and t_s and t_p are the Fresnel transmission coefficients. We use Eq. (4) to fit the photocurrent (black line in Fig. 2) and extract the CPGE (red dashed line) and LPGE (blue line) contributions. The amplitudes of the two contributions are presented in Table I at zero and finite applied magnetic field.

The observation of the CPGE can therefore be explained in terms of Rashba SO coupling and the formation of a spin helix texture in the $(10\bar{1}0)$ interface plane. The interband optical transitions excited by the circularly polarized light result in a deterministic selection of electron spin due to optical selection rules and in the creation of photoelectrons and photoholes. Note that the photoholes are quickly compensated due to the high concentration of donors and can be neglected in the analysis of the photocurrent effect. The photoelectrons are asymmetrically distributed in k space and thereby generate an effective current, which depends on the helicity of the incident light. For a detailed explanation of the effect, we refer the reader to the review papers by Ganichev and Prettl [30] and Ivchenko [31].

To investigate the spin texture and its coupling to the orbital momentum, we apply an external magnetic field in the plane of the persistent spin helix $(10\bar{1}0)$ parallel and perpendicular

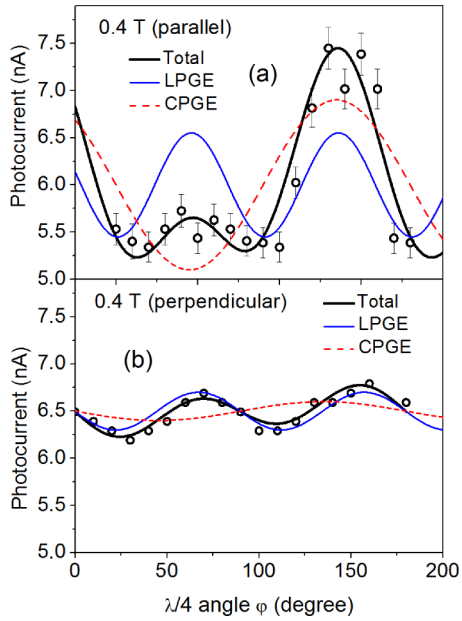

FIG. 3. Photocurrent of sample ZLH measured while applying an external magnetic field of 0.4 T in the $(10\bar{1}0)$ plane (a) parallel and (b) perpendicular to the y direction (circles). The thick black line represents the fit to Eq. (3), with the parameters defined in Table I. The thin dashed red line represents the CPGE contribution to the photocurrent as extracted from the fit and the thin blue line represents the LPGE contribution.

to the y axis, the current direction. Figure 3(a) shows the PGE measured under an applied magnetic field of 0.4 T, parallel to the y axis. The CPGE contribution is twice as large as that measured without applied field. On the other hand, Fig. 3(b) shows a clear reduction of the CPGE current in y direction, when an in-plane magnetic field of 0.4 T is applied perpendicular to the y axis, i.e., in x direction.

This observation can be explained in terms of the spin texture near the valence band maximum shown in Fig. 3(a) in the paper of Absor *et al.* [23]. The applied magnetic field B introduces an additional spin dependent term in the Hamiltonian, accounting for the Zeeman interaction:

$$H_Z = \frac{g\mu_B}{2\hbar}\boldsymbol{\sigma} \cdot \boldsymbol{B}, \quad (5)$$

which results in an additional splitting of the spin subbands. By applying the magnetic field in y direction, the Zeeman interaction term enhances the spin-subband splitting for $k_x \neq 0$, whereas a magnetic field of 0.4 T applied in x direction destroys the spin helix texture and the spin subbands become symmetric in k space, inducing a clear decrease of the CPGE current.

Finally, we would like to note that the formation of the interface in the $(10\bar{1}0)$ plane is possible thanks to the Li dopants that stabilize the Zn vacancies (V_{Zn}) and V_{Zn}-HO complexes, produced by the proton implantation from a polarized interface [32,33]. This gives rise to the spin helix by Rashba coupling [24]. In the absence of Li dopants, which is the case of the pure ZnO sample even after proton implantation, the lower stability of the V_{Zn} defects prevents the formation of stable V_{Zn}-HO complexes and therefore the formation of the interface, which

explains the lack of CPGE in sample ZH. In sample ZFH, the high concentration of intrinsic donor defects throughout the sample prevents the formation of the 2D interface.

IV. CONCLUSIONS

In conclusion, we showed that a large Rashba SOI is present in the 2DEG built at the interface of a semiconductor/insulator homojunction parallel to the $(10\bar{1}0)$ surface of a ZnO:Li microwire, as predicted by Absor *et al.* [23]. We demonstrated that the anisotropy of SO coupling can be probed through measurement of the circular photogalvanic effect and provided a technique for tuning the Rashba SOI by changing the orientation of an external magnetic field in the plane of the interface. Finally, the presented results indicate the realization of a persistent spin helix at the interface plane, which could open new paths for spintronic applications in ZnO-based materials.

Further studies are necessary to investigate the dynamics of the spin texture. A more detailed analysis of the texture in the presence of small ($B << 0.4$ T) applied magnetic fields are of great interest, especially because the near surface states between the interface containing the 2DEG and the sample surface are known to be magnetically ordered [32].

ACKNOWLEDGMENTS

This work was supported by the Collaborative Research Center (SFB762) "Functionality of Oxide Interfaces" (DFG). Y.K. was partially supported by the Department of Science and Technology, India [DST/INSPIRE/04/2015/002938]. Discussions with W. Hergert and V. Brosco are gratefully acknowledged.

[1] G. Dresselhaus, Phys. Rev. **100**, 580 (1955).
[2] E. I. Rashba, Sov. Phys. Solid State **2**, 1109 (1960).
[3] B. A. Bernevig, J. Orenstein, and S.-C. Zhang, Phys. Rev. Lett. **97**, 236601 (2006).
[4] J. D. Koralek, C. P. Weber, J. Orenstein, B. A. Bernevig, S. C. Zhang, S. Mack, and D. D. Awschalom, Nature (London) **458**, 610 (2009).
[5] A. Sasaki, S. Nonaka, Y. Kunihashi, M. Kohda, T. Bauernfeind, T. Dollinger, K. Richter, and J. Nitta, Nat. Nanotechnol. **9**, 703 (2014).
[6] S. Datta and B. Das, Appl. Phys. Lett. **56**, 665 (1990).
[7] H. C. Koo, J. H. Kwon, J. Eom, J. Chang, S. H. Han, and M. Johnson, Science (NY) **325**, 1515 (2009).
[8] K. C. Nowack, F. H. L. Koppens, Y. V. Nazarov, and L. M. K. Vandersypen, Science **318**, 1430 (2007).
[9] S. Nadj-Perge, S. M. Frolov, E. P. Bakkers, and L. P. Kouwenhoven, Nature (London) **468**, 1084 (2010).
[10] J. W. G. van den Berg, S. Nadj-Perge, V. S. Pribiag, S. R. Plissard, E. P. A. M. Bakkers, S. M. Frolov, and L. P. Kouwenhoven, Phys. Rev. Lett. **110**, 066806 (2013).
[11] Y. Xie, L. Zhang, Y. Zhu, L. Liu, and H. Guo, Nanotechnology **26**, 455202 (2015).
[12] Q. Zhang, X. Q. Wang, X. W. He, C. M. Yin, F. J. Xu, B. Shen, Y. H. Chen, Z. G. Wang, Y. Ishitani, and A. Yoshikawa, Appl. Phys. Lett. **95**, 031902 (2009).
[13] V. K. Dugaev, M. Inglot, E. Y. Sherman, and J. Barnaś, Phys. Rev. B **82**, 121310 (2010).
[14] N. Ogawa, M. S. Bahramy, Y. Kaneko, and Y. Tokura, Phys. Rev. B **90**, 125122 (2014).
[15] M. Inglot, V. K. Dugaev, E. Y. Sherman, and J. Barnaś, Phys. Rev. B **91**, 195428 (2015).
[16] J. Nitta, T. Akazaki, H. Takayanagi, and T. Enoki, Phys. Rev. Lett. **78**, 1335 (1997).
[17] L. Meier, G. Salis, I. Shorubalko, E. Gini, S. Schön, and K. Ensslin, Nat. Phys. **3**, 650 (2007).
[18] T. Y. Lee, J. Chang, M. C. Hickey, H. C. Koo, H.-j. Kim, S. H. Han, and J. S. Moodera, Appl. Phys. Lett. **98**, 202504 (2011).
[19] Y. H. Park, H.-j. Kim, J. Chang, S. H. Han, J. Eom, H.-J. Choi, and H. C. Koo, Appl. Phys. Lett. **103**, 252407 (2013).
[20] Y. F. Hao, Eur. Phys. J. B **85**, 84 (2012).
[21] Q. Zhang, X. Q. Wang, C. M. Yin, F. J. Xu, N. Tang, B. Shen, Y. H. Chen, K. Chang, W. K. Ge, Y. Ishitani, and A. Yoshikawa, Appl. Phys. Lett. **97**, 041907 (2010).
[22] J. X. Duan, N. Tang, J. D. Ye, F. H. Mei, K. L. Teo, Y. H. Chen, W. K. Ge, and B. Shen, Appl. Phys. Lett. **102**, 192405 (2013).
[23] M. A. U. Absor, F. Ishii, H. Kotaka, and M. Saito, Appl. Phys. Express **8**, 073006 (2015).
[24] M. A. U. Absor, F. Ishii, H. Kotaka, and M. Saito, AIP Adv. **6**, 025309 (2016).
[25] S. D. Ganichev and L. E. Golub, Phys. Status Solidi (b) **251**, 1801 (2014).
[26] C. Yin, B. Shen, Q. Zhang, F. Xu, N. Tang, L. Cen, X. Wang, Y. Chen, and J. Yu, Appl. Phys. Lett. **97**, 181904 (2010).
[27] V. V. Bel'kov, S. D. Ganichev, P. Schneider, C. Back, M. Oestreich, J. Rudolph, D. Hägele, L. E. Golub, W. Wegscheider, and W. Prettl, Solid State Commun. **128**, 283 (2003).
[28] I. Lorite, C. Zandalazini, P. Esquinazi, D. Spemann, S. Friedländer, A. Pöppl, T. Michalsky, M. Grundmann, J. Vogt, J. Meijer, S. P. Heluani, H. Ohldag, W. A. Adeagbo, S. K. Nayak, W. Hergert, A. Ernst, and M. Hoffmann, J. Phys.: Condens. Matter **27**, 256002 (2015).
[29] I. Lorite, Y. Kumar, P. Esquinazi, C. Zandalazini, and S. P. de Heluani, Small **11**, 4403 (2015).
[30] S. D. Ganichev and W. Prettl, J. Phys.: Condens. Matter **15**, R935 (2003).
[31] E. L. Ivchenko, Phys. Usp. **45**, 1299 (2007).
[32] I. Lorite, B. Straube, H. Ohldag, P. Kumar, M. Villafuerte, P. Esquinazi, C. E. R. Torres, S. P. d. Heluani, V. N. Antonov, L. V. Bekenov, A. Ernst, M. Hoffmann, S. K. Nayak, W. A. Adeagbo, G. Fischer, and W. Hergert, Appl. Phys. Lett. **106**, 082406 (2015).
[33] N. T. Son, J. Isoya, I. G. Ivanov, T. Ohshima, and E. Janzén, J. Phys.: Condens. Matter **25**, 335804 (2013).